frontiers | Frontiers in Marine Science

TYPE Original Research
PUBLISHED 28 August 2025
DOI 10.3389/fmars.2025.1627553



OPEN ACCESS

EDITED BY
Fei Li,
Southwest Petroleum University, China

REVIEWED BY
Lijing Liu,
Northwest University, China
Fan Wei,
Yunnan University, China

*CORRESPONDENCE
Yi-jiang Zhong
zhongyijiang2012@cdut.edu.cn

RECEIVED 13 May 2025
ACCEPTED 04 August 2025
PUBLISHED 28 August 2025

CITATION
Zhong Y-j, Liu G, Dong Y-x and Algeo TJ (2025) Calcified cyanobacteria from the Upper Ediacaran of South China. *Front. Mar. Sci.* 12:1627553. doi: 10.3389/fmars.2025.1627553



# Calcified cyanobacteria from the Upper Ediacaran of South China

Yi-jiang Zhong[1,2]*, Gang Liu[1,2], Yi-xin Dong[1] and Thomas J. Algeo[1,2,3,4]

[1]State Key Laboratory of Oil and Gas Reservoir Geology and Exploitation, Chengdu University of Technology, Chengdu, China, [2]Institute of Sedimentary Geology, Chengdu University of Technology, Chengdu, China, [3]Department of Geosciences, University of Cincinnati, Cincinnati, OH, United States, [4]State Key Laboratories of Geomicrobiology and Environmental Changes (GMEC) & Geological Processes and Mineral Resources (GPMR), China University of Geosciences, Wuhan, China

Fossil records of calcified cyanobacteria from the Neoproterozoic are rare despite the high carbonate saturation of contemporaneous seawater. In this study, we report the discovery of calcified cyanobacteria in microbialites from the Upper Ediacaran Dengying Formation in South China, based on integrated field investigations and petrographic analyses of polished surfaces and thin-sections. Scanning electron microscopy (SEM), energy-dispersive X-ray spectroscopy (EDS), and X-ray diffraction (XRD) reveal that filamentous sheath structures are preserved as dense, fine-crystalline dolomite. The tube-like microfossils are identified as the calcified cyanobacteria *Girvanella*. This discovery fills a gap in the fossil record of microbialite-hosted calcified cyanobacteria spanning the interval from the Cryogenian glaciations to the onset of the Cambrian Period. Petrographic and mineralogical analyses indicate that primary high-Mg calcite, precipitated *in vivo* within *Girvanella* sheaths as a likely precursor to microcrystalline dolomite, contributed to the exceptional preservation of these fossils. The sporadic occurrence of calcified cyanobacteria may reflect transient episodes of elevated carbonate saturation driven by fluctuations in seawater chemistry. Concurrently, the possible rapid evolution of $CO_2$-concentration mechanisms (CCMs) may have enhanced the calcification capability of cyanobacteria. Thus, these features foreshadowed the widespread microbial calcification that emerged in the Cambrian.

KEYWORDS

**Denying Formation, *Girvanella*, extracellular polymeric substances, dolomite, Neoproterozoic, calcification, $CO_2$-concentration mechanism**

## 1 Introduction

Cyanobacteria are prokaryotic organisms that appeared by ~3.5 Ga (Merz-Preiβ, 2000; Altermann et al., 2006). They drive much of the Earth's biological productivity (Lochte and Turley, 1988), and, as the most abundant photoautotrophs of the Proterozoic (Schirrmeister et al., 2015), they generated most of the planet's early oxygen reservoir (Brocks et al., 2003a, b; Jansson and Northen, 2010). Cyanobacterial biomineralization is a

major process in the global carbon cycle (Ridgwell and Zeebe, 2005), in which $CO_2$ is fixed through *in vivo* sheath calcification (Riding, 2006; Altermann et al., 2006; Kah and Riding, 2007; Jansson and Northen, 2010; Kamennaya et al., 2012). These processes played a fundamental role in shaping the long-term evolution of the Earth's atmosphere and hydrosphere (Riding, 2011; Demoulin et al., 2019).

Cyanobacterial biomineralization forms a range of carbonate fabrics, including most Precambrian microbialites (Riding, 2006; Altermann et al., 2006; Kah and Riding, 2007; Jansson and Northen, 2010; Kamennaya et al., 2012). Almost all cyanobacterial fossils of that age are preserved in chert (Schirrmeister et al., 2016; Demoulin et al., 2019; Manning-Berg et al., 2019), shale (Woltz et al., 2021), or phosphate (Sisodia, 2009). Although microbialites are highly abundant in Precambrian rocks, fossil records of calcified cyanobacteria are rare. The paucity of calcified cyanobacteria prior to the Neoproterozoic (Swett and Knoll, 1985; Knoll et al., 1993; Turner et al., 1993, 2000), despite the high $CaCO_3$ saturation state of contemporaneous seawater (Knoll et al., 1993), is known as the 'Precambrian Enigma' (Riding, 1994).

The earliest definitively identified calcified sheaths of the cyanobacterium *Girvanella* date to ~750-700 Ma (Swett and Knoll, 1985), although rare calcified fossils tentatively assigned to this genus have been reported from pre-Cryogenian strata (i.e., ~1200 Ma, Kah and Riding, 2007; ~1083-799 Ma, Turner et al., 1993). Global cooling during the Cryogenian 'Snowball Earth' events, i.e., the Sturtian (~717-659 Ma) and Marinoan (~649/639-635 Ma) ice ages (Hoffman et al., 2017; see Yu et al., 2020 re Cryogenian glacial terminology), may have hindered cyanobacterial calcification (Riding, 2006). However, it is not clear why fossils of calcified cyanobacteria are rare in the Ediacaran as increasing temperature and decreasing atmospheric $CO_2$ in the aftermath of the Snowball Earth glaciations would have generated conditions suitable for cyanobacterial calcification (Riding, 2006; Min et al., 2020). Recently, phosphatized calcified cyanobacteria were identified in the Gaojiashan Member of the Dengying Formation in southern Shanxi Province, South China (Min et al., 2019, 2020). Although this discovery serves as indirect proof of cyanobacterial calcification during the late Ediacaran, direct proof in the form of calcified fossils of sheath cyanobacteria is still lacking.

The main goal of this study was to search for evidence of calcified cyanobacteria in microbialites of the Upper Ediacaran Dengying Formation. For this purpose, we conducted sedimentological investigations of two field sections (Xianfeng and Shizhu) featuring microbialites in the Dengying Formation of the southwestern Sichuan Basin of South China (Figure 1). Through detailed field studies and petrographic analyses of polished surfaces and thin-sections ($n$ = 43), fossils of calcified cyanobacteria were found in four samples (Samples I to IV). Furthermore, we carried out scanning electron microscopic (SEM) imaging, energy-dispersive X-ray spectroscopy (EDS) measurements, and X-ray diffraction (XRD) analysis to show that the filament sheaths of the calcified cyanobacteria are preserved in the form of dense, fine dolomite. The results of the present study fill a gap in the fossil record of calcified cyanobacteria during the late Neoproterozoic, potentially shedding new light on the 'Precambrian Enigma'. The findings also contribute important biological evidence regarding microbial mat ecosystems, cyanobacterial calcification mechanisms, and shifts in marine chemical conditions during the Ediacaran-Cambrian (E-C) transition.

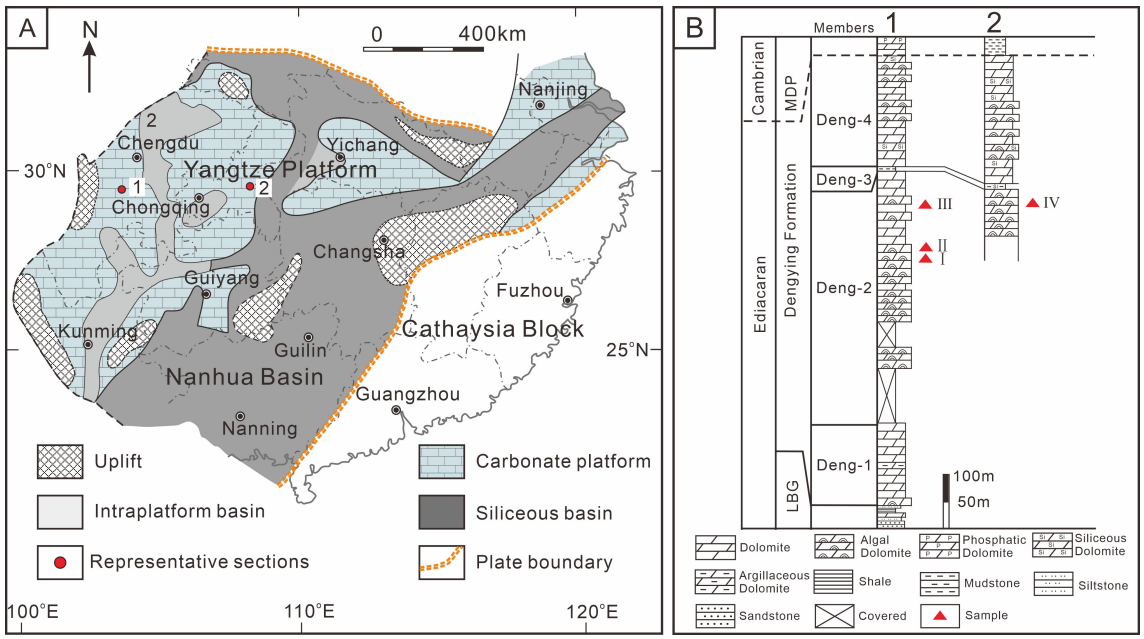


FIGURE 1
**(A)** Location of study sections (1 = Xianfeng, 2 = Shizhu) containing calcified cyanobacterial fossils. **(B)** Measured sections of Dengying Formation in the Xianfeng section. LBG, Labagang Formation; MDP, Maidiping Formation.

## 2 Geological setting

The Upper Ediacaran Dengying Formation of the Sichuan Basin, South China is dominated by dolostone that ranges from non-fossiliferous to microbial (the latter formerly termed "algal dolostone"), has been dated to 551 ± 0.7 Ma to 538.8 ± 0.2 Ma (Condon et al., 2005; Cohen et al., 2023). It conformably overlies the Labagang Formation, the top of which is marked by black shale, and is separated from the overlying Maidiping Formation by a parallel unconformity (Deng et al., 2015). The E-C boundary is readily recognized on the Yangtze Platform by a lithological change from dolostone-dominated Upper Ediacaran strata to the phosphorite-chert succession of the basal Cambrian (Cai et al., 2011). The sedimentary environment of the Dengying Formation was a restricted shallow-marine carbonate platform (Shi et al., 2013) that developed over a Neoproterozoic rifted continental margin (Jiang et al., 2008). Microbialite, i.e., an *in situ* laminated organo-sedimentary structure formed in part by the metabolic activities of microorganisms such as cyanobacteria (Fang et al., 2003; Lin et al., 2017; Dupraz et al., 2009), is abundant in intra-platform bioherms (Zhou et al., 2017) and tidal mats (Song et al., 2017) of the Dengying Formation. This formation can be divided into four members based on microbialite abundance. Microbialites are rare in the lowermost Deng-1 Member, which mainly comprises unfossiliferous dolostone, and in the thin (3 m) Deng-3 Member, composed of blue-gray to dark gray siliciclastic rocks. In contrast, they are abundant in the Deng-2 and Deng-4 members, both dominated by algal dolostone (Figure 1). Calcified cyanobacteria were discovered in the upper part of the Deng-2 Member of the Dengying Formation, which represents deposits on a shallow-marine carbonate platform.

## 3 Methods and samples

Forty-three fresh samples were collected from the Deng-2 Member of the Dengying Formation of the Xianfeng and Shizhu sections and sawn open perpendicular to the bedding direction. One half was polished using a polishing machine, and the other half was used in thin-section preparation. The uncovered thin-sections were examined using a Nikon Optiphot 2-POL optical microscope equipped with a CM2000 digital camera and Imageview imaging software, to examine petrographic features. Samples I to IV yielded evidence of calcified cyanobacteria, and these thin-sections were then prepared for SEM analysis. Both the thin-section and SEM analysis were conducted at the State Key Laboratory of Oil and Gas Reservoir Geology and Exploitation in the Chengdu University of Technology. The locations of fossils in the thin-sections were marked with a black permanent marker under the optical microscope for easy location during SEM analysis. An ultra-thin coating (ca. 10 nm) of gold was then deposited on the marked thin-sections by low vacuum sputter coating. SEM imaging and energy-dispersive X-ray spectroscopy (EDS) measurements were performed using a ZEISS Sigma 300 SEM with an integrated EDS detector (Bruker Quantax 200 with X Flash 630 Detector). Samples were imaged using secondary electrons, and the Atomic Number, Absorption and Fluorescence effect (ZAF) correction method was used for semiquantitative results. Forty-two SEM images were obtained to check the microstructures of the fossils. EDS measurements were performed at 10 kV accelerating voltage with a working distance of 7.1 mm, with results calculated as both quantity % and atomic %. Bulk samples of ~10 g weight were split from the unpolished half of each sample, gently crushed, and ground to a ~200-mesh powder using an agate pestle and mortar. XRD analyses were carried out at Sichuan Keyuan Testing Center of Engineering Technology Limited Liability Company with a PANalytical Empyrean powder-ray diffractometer using the quantitative analysis method of diffraction peak integration intensity to generate X-ray diffraction spectra.

## 4 Results

### 4.1 Meso-structures

Samples I and II exhibit parallel mm-scale laminae that are generally laterally continuous and densely spaced in the vertical direction (Figures 2A, C). The laminae are straight or slightly wavy, with the individual undulations of the latter being 1-2 mm in length and 0.5-1.5 cm in height. In each sample, dark microcrystalline layers alternate with light layers composed of more coarsely crystalline material, both layer types showing uneven thicknesses ranging from 0.5 to 1 cm (Figures 2A, C). Tube-like microfossils were observed in the upper laminae of Sample I and between the laminae of Sample II. At higher magnification, it was observed that the dark layers are thicker than the light layers (Figures 2B, D). The samples also exhibit abundant vugs filled with drusy dolomite in irregular shapes (Figures 2B, D).

Sample III consists of two sediment layers that are separated by a scoured surface (Figure 3A). The lower unit consists of dark-colored peloidal dolomite, whereas the upper unit consists of crystalline dolomite and sparry cement showing a reduced abundance of dark-colored clasts up section. The dark-colored clasts are fragments of the lower peloidal dolomite, broken up by high-energy processes. The cyanobacterial fossils examined in this study are present above the irregular surface (Figure 3A). This clastic layer is approximately 1 cm thick and is characterized by a layer filled with light-colored cement clasts and dark-colored microbial clasts (Figure 3B). The clasts are irregular in shape and exhibit various sizes and shapes, with the dark-colored clasts generally being ovate and the light-colored clasts rodlike to ovate. All of the clasts probably represent rip-up clasts from the underlying sediment layer.

Sample IV is a typical stromatolite, composed of overlapping and undulating layers of light and dark layers that exhibit convex upward curvature. Compared to Samples I and II, Sample IV has a more regularly layered structure. Voids filled with white coarse crystalline cement are common, especially in areas of upward-arching microbial laminae (Figures 4A, B). The dark layers exhibit horizontal continuity with few interruptions. At higher magnification, it can be observed that the dark layers, which have

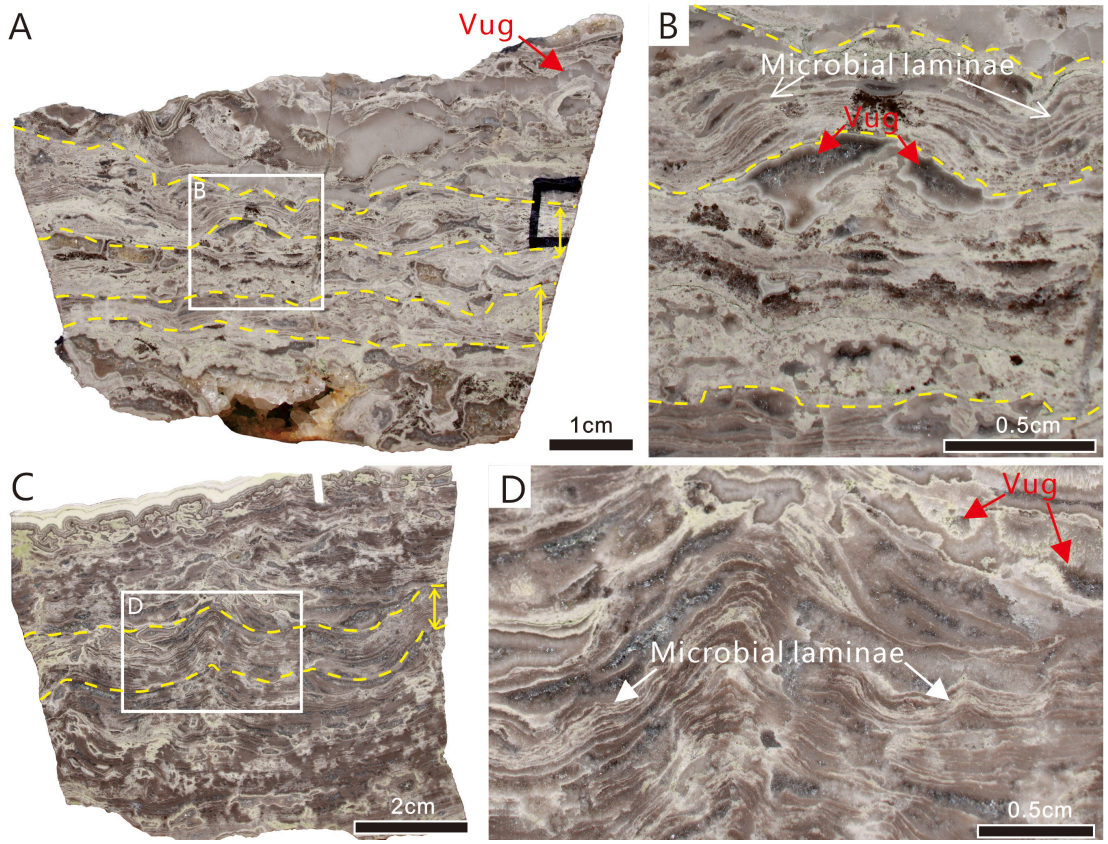


FIGURE 2
Reflected light photographs of polished slabs showing meso-structure of microbial laminae containing calcified cyanobacterial fossils (toward the upper layer of the rock). **(A)** Sample I, two layers of dense parallel superposed laminae (between the yellow solid lines as indicated by the yellow double-sided arrows on the right) alternate with a layer rich in cement-filled primary vugs. **(B)** Close-up of area of dotted rectangle in A. **(C)** Sample II, which has similar character to Sample I. **(D)** Close-up of area of dotted rectangle in **(C)** Scale bars: A = 1 cm; B, C = 0.5 cm; D = 2 cm.

thicknesses >2 mm, exhibit a uniformly dense structure without visible finer laminae (Figure 4B). The tube-like microfossils are present in the dark layers.

## 4.2 Microstructures

### 4.2.1 Microstructures of Samples I and II

The main petrographic feature of Samples I and II is a lamelliform fabric consisting of alternating dark-colored microcrystalline and light-colored more coarsely crystalline laminae (Figures 5, 6). The white laminae are 50-200 μm in thickness and laterally continuous. The dark laminae have thicknesses exceeding 100 μm and contain abundant thin-walled tube-like microfossils. The tube-like microfossils, which are restricted to the thinner laminae that consist of a denser microcrystalline material, are unevenly distributed within each lamina (Figures 5B, E, 6B, D). Laterally within an individual dark lamina, fossil outlines become vaguer as the lamina becomes interrupted by irregular light plaques (white arrows in Figures 5A, D). Alternating with the dark laminae, the light laminae are characterized by less continuous lateral extents and frequent interruptions by patches of dark microcrystalline material.

The tube-like microfossils consist of an outer filament sheath of darker material around a clear (microcement-filled) interior. Individual sheaths have uniform external diameters of approximately 30 μm and smooth surfaces, with uniformly thin walls and open ending. The walls consist of dark gray microcrystals, whereas the interior of the tube consists of a more coarsely crystalline dolomite cement (Figures 5C, F, 6B, D). The tube-like fossils typically occur as dense clusters, tangled together irregularly (Liu et al., 2016; Riding, 2011; Mei et al., 2021), yet they are never twisted together into nodules. The intersection of the thin-section plane with the tubular fossils yields cross-sections ranging from round to elliptical, reflecting the tubular structure of these organisms. Most tubes have an axial length of less than 100 μm, with the longest being ~200 μm (Figure 5B). The interiors of the tubes are devoid of any visible organs, axial walls, or other features. Individual tubes are interwoven horizontally and obliquely, reflecting prostrate growth in the form of a filament sheet. Erect filaments (i.e., with growth perpendicular to bedding) are rare. These microfossils consist of non-tapering, unbranched or presence of false branched (white arrows in Figure 5F), relatively straight or slightly sinuous microcrystalline tubules and are generally surrounded by microcrystalline cement.

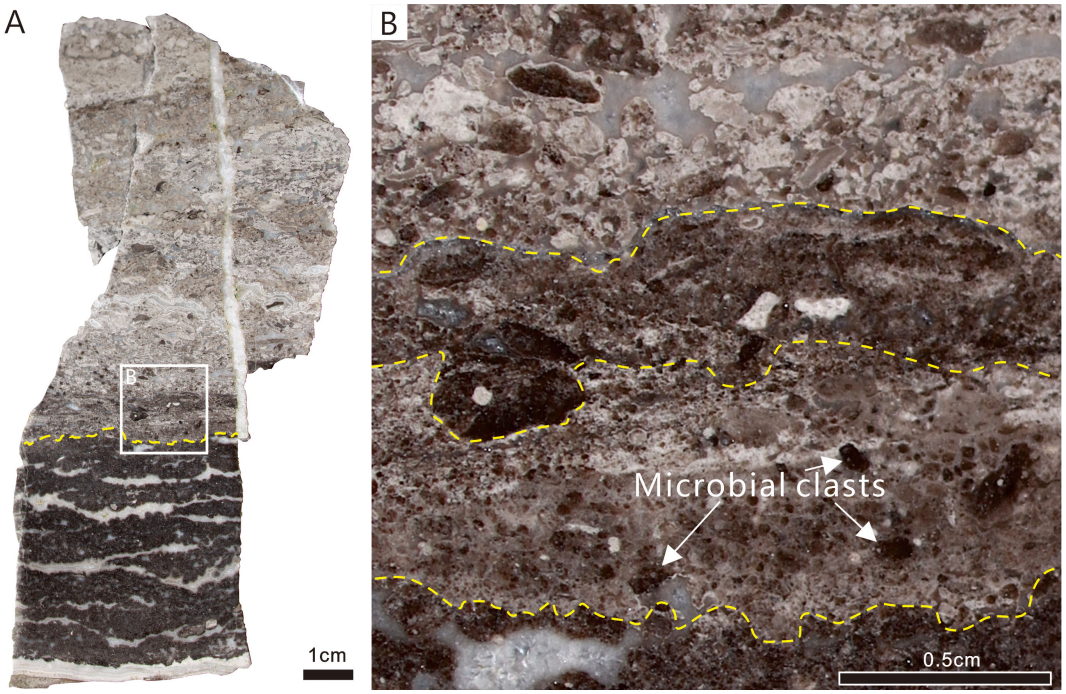


FIGURE 3
Reflected light photographs of polished slabs showing meso-structure of microbial clasts containing calcified cyanobacterial fossils (toward the upper layer of the rock). **(A)** Sample III, two sedimentary microfacies, divided by a scoured surface (yellow dotted line). Solid line illustrates the boundaries of the microfacies. **(B)** Close-up of area of dotted rectangle in **(A)** Scale bars: A = 1 cm; B = 0.5 cm.

### 4.2.2 Microstructures of Sample III

Microstructures of Sample III, under the optical microscope, are characterized by rip-up intraclasts surrounded by a thin fringe of isopachous fibrous dolomite cement, embedded in bright crystalline coarse-grained dolomite (Figure 7A). The clasts mainly consist of masses of tube-like microfossils and dark dense microcrystalline cement. They have distinctive and regular margins and vary in diameter from < 100 μm to 1 mm. The clasts exhibit a variety of shapes, including roughly circular, or elongate, oval, and irregular. Generally, the smaller clasts are more circular, while larger clasts have more irregular or elongate shapes. Meanwhile, the bar- and oval-shaped clasts do not exhibit any directional arrangement.

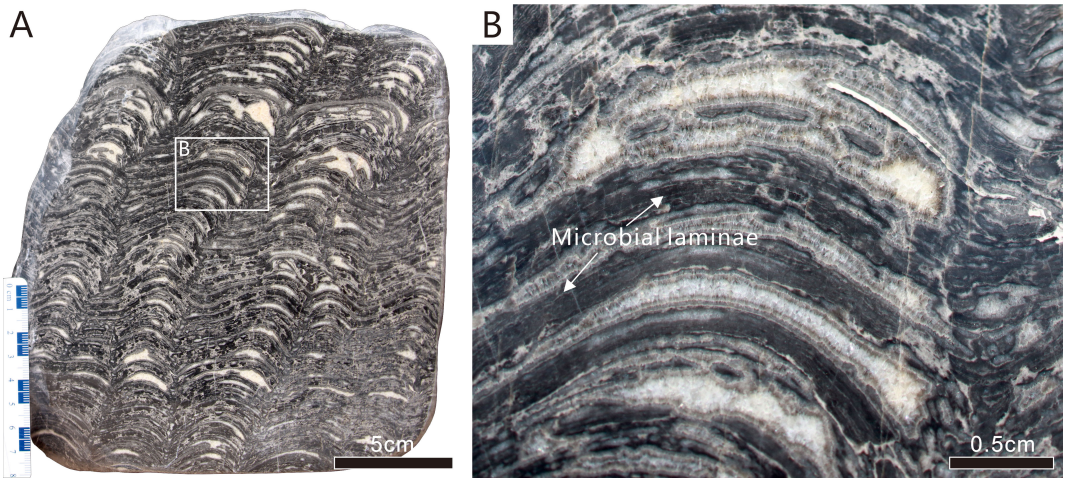


FIGURE 4
Reflected light photographs of polished slabs showing meso-structure of microbial laminae containing calcified cyanobacterial fossils (toward the upper layer of the rock). **(A)** Sample IV, stromatolite with undulating layers, wide crests and sharp troughs. **(B)** Close-up of area of solid rectangle in **(A)** Scale bars: A = 5 cm; B = 0.5 cm.

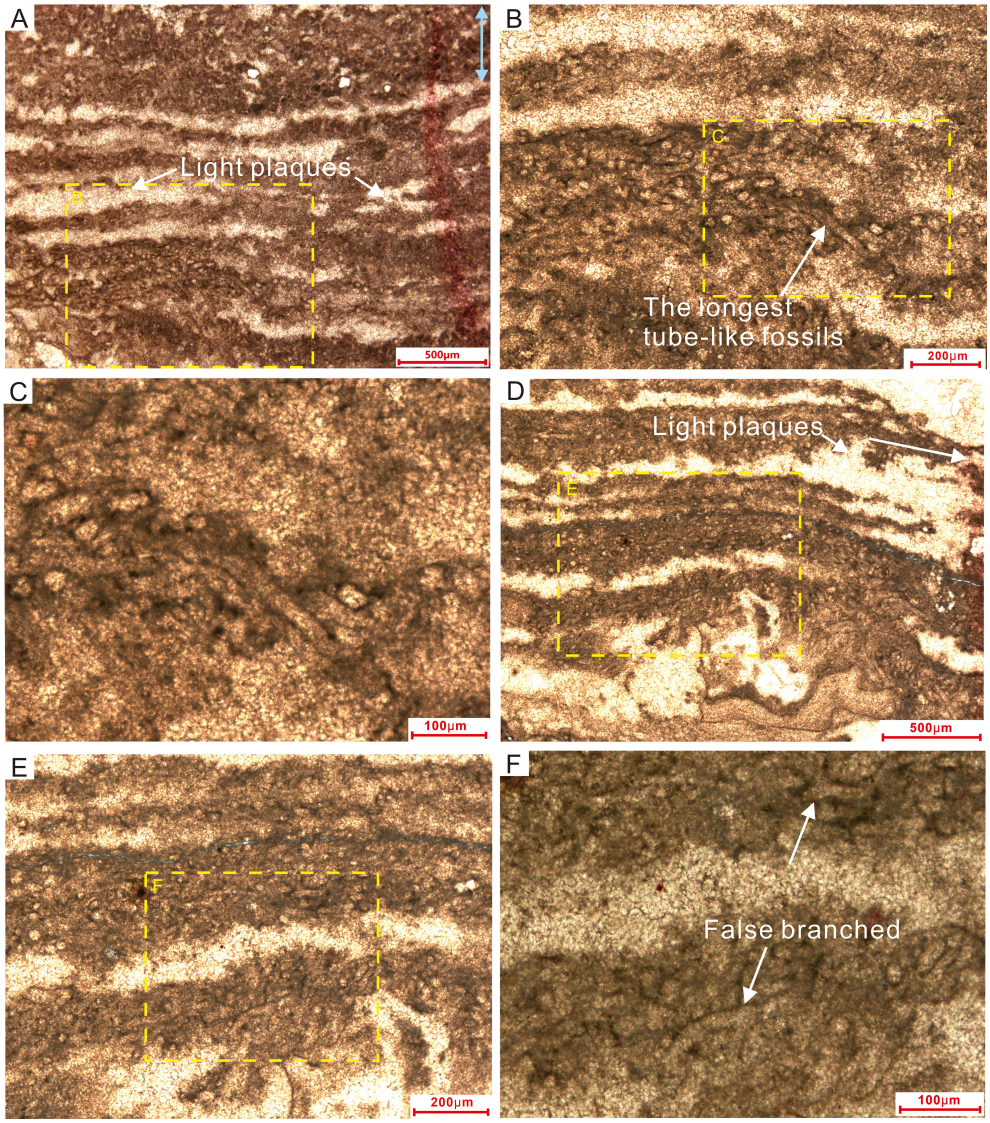


FIGURE 5
Thin-section microphotographs of laminated microstructures in Sample I. **(A, D)** Dense dark microcrystalline laminae alternating with light-colored more coarsely crystalline material. The tube-like microfossils are distributed unevenly within the dark laminae. **(B, C, E, F)** Magnified views of the laminae, highlighting details of the tube-like microfossils. Dotted rectangles in **(A, B)** show the areas of **(B, C)**, respectively; likewise for **(D–F)**.

The clasts have been partly or wholly recrystallized to a bright crystalline material with planar to subangular shapes (Figure 7A). The wholly recrystallized clasts exhibit thin microcrystalline rims.

The external diameters of the filaments in Sample III are nearly the same as those of the fossils in Sample I. The fossils with round or oval shapes in cross-section, which might be coccoid cyanobacteria, are densely distributed in the central area (Figure 7B) and randomly scattered throughout the matrix. In the outer part of the clasts, curved tubules more than 1 mm in length lie parallel to the outer margin of the clasts, forming an outer multilayer envelope (Figure 7B). The tails of the elongate clasts are mostly lacking round or oval tubules, although they contain curved tubules parallel to the margins or the axial direction (Figure 7A). The presence of the curved tubules, forming an envelope around the clasts, controls whether the margins are regular or irregular. Moreover, the internal diameters of the curved tubules, which are filled with bright microcrystalline carbonate, are greater than those of the round or oval tubules.

### 4.2.3 Microstructures of Sample IV

The laminae (lamelliform fabric) texture of Sample IV consists of alternating dark dense microcrystalline material and more coarsely crystalline white material (Figure 8). The width of the white laminae varies inconsistently, often interrupted by microcrystalline structures, leading to discontinuities within individual laminae. Some of the boundaries between the dark and white layers are also blurred. The tube-like microfossils are randomly located within the densest part of the laminae, which is composed mainly of microcrystalline material. The individual attributes, encompassing size and morphology, as well as the

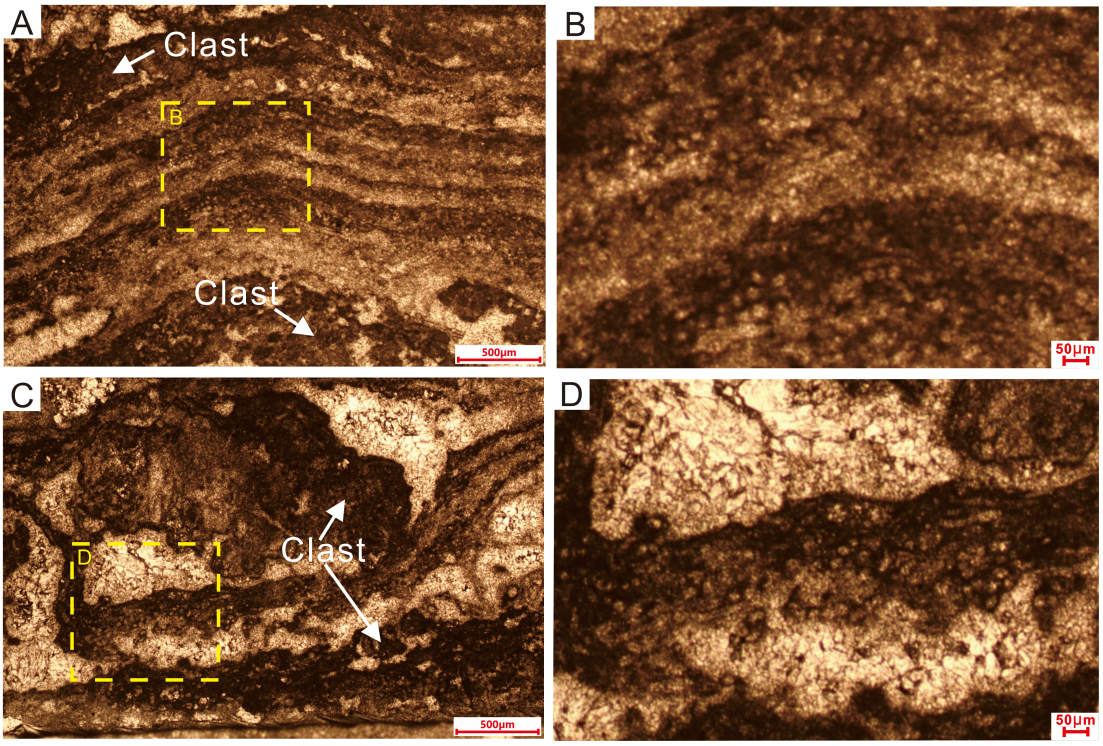


FIGURE 6
Thin-section microphotographs of laminated microstructures in Sample II. **(A)** Dense dark microcrystalline laminae alternating with light-colored more coarsely crystalline material. The tube-like microfossils are distributed unevenly within the dark laminae. White arrows in **(A, C)** show clasts without any tube-like microfossils. **(B, D)** Magnified views of the laminae, highlighting details of the tube-like microfossils. Dotted rectangles in **(A, C)** represent the areas of **(B, D)**, respectively.

collective structural arrangement of these fossils, closely resemble those exhibited by Samples I and II (Figure 8).

### 4.2.4 Microstructures under SEM

Filament sheaths, which appear as dark gray microcrystalline material (Figures 9A, B, G, H) under the optical microscope, are defined by dense and fine dolomite crystals under the SEM (Figures 9C–E, I–K). The microcrystalline dolomite is made up of euhedral rhombs with planar surfaces, which vary in size from < 2 μm to nearly 5 μm across (Figures 9E, K). The irregular microcrystalline filling between or inside the cylinders has variable crystal sizes of up to 10 μm. EDS analyses of fine crystals in the sheaths (Figures 9F, L) revealed a chemical composition of nearly 50 mol% $MgCO_3$ and 50 mol% $CaCO_3$, which verifies their dolomitic mineralogy. The high

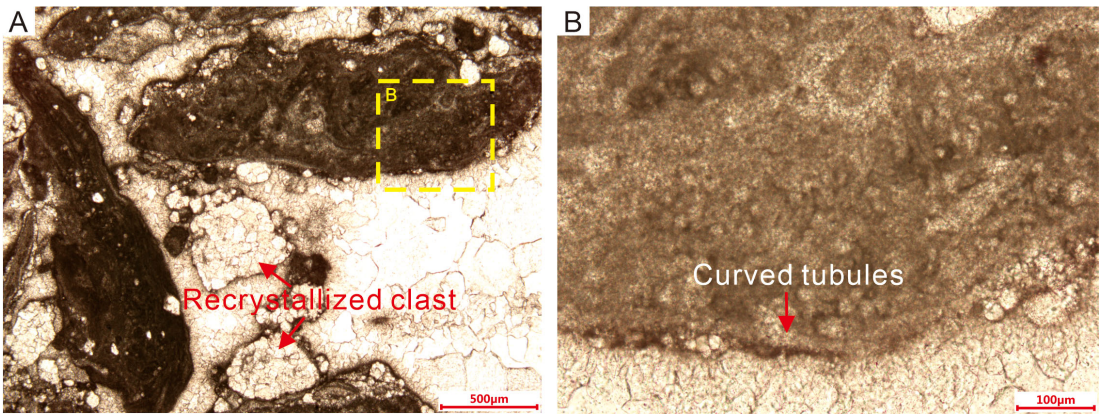


FIGURE 7
Thin-section microphotographs of clasts and microstructures in Sample III. **(A)** The clasts are mainly composed of dense dark microcrystalline material alternating with light-colored more coarsely crystalline material between the clasts. The tube-like microfossils are distributed unevenly within the clasts. **(B)** Magnified view of a clast, highlighting details of the tube-like microfossils.

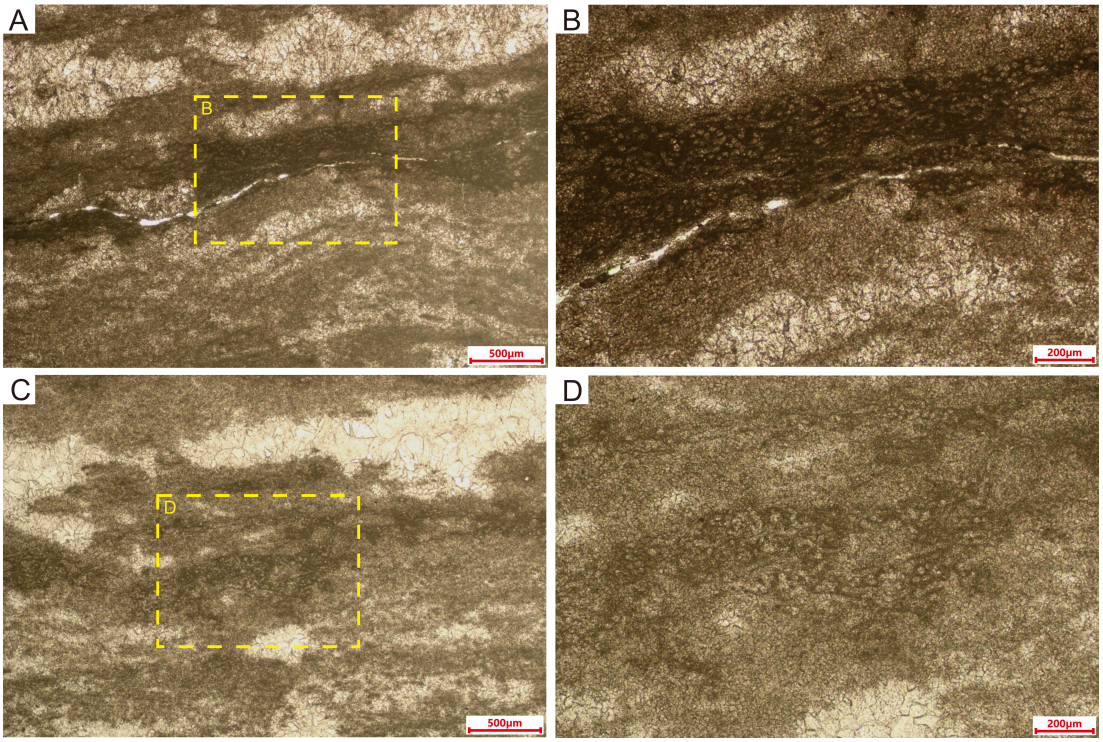


FIGURE 8
Thin-section microphotographs of laminated microstructures in Sample IV. **(A, C)** Alternating light and dark layers, with tube-like microfossils best preserved in the densest (darkest) part of dark layers. **(B, D)** Magnified views of laminae, highlighting details of the tube-like microfossils.

carbon content (59.2% and 54.3%) indicates abundant organic matter within the calcified filament sheaths. Furthermore, the Ca-Mg carbonate material was classified as having an almost dolomitic composition through XRD analyses, which show a superstructure with crystal planes at 101, 015, and 021 (Figure 10).

# 5 Discussion

## 5.1 Calcified cyanobacteria in the Precambrian

According to empirical and modelled paleo-atmospheric estimates, atmospheric partial pressures of $CO_2$ ($pCO_2$) were below ~0.4% (= 4000 ppm) at 1200-700 Ma, equivalent to no more than 10 times present atmospheric level (10 PAL) (Riding, 2006). Global cooling during the Cryogenian 'Snowball Earth' period, which comprised the Sturtian and Marinoan ice ages (Hoffman et al., 2017; Yu et al., 2020), may have temporarily halted the development of CCMs and hindered cyanobacterial calcification (Riding, 2006). However, it is not clear why Calcified cyanobacterial fossils are rare in the interval between the termination of Cryogenian ice ages and the Precambrian-Cambrian transition (i.e., the Ediacaran Period) as increases in temperature and decreases in $pCO_2$ would have generated conditions suitable for CCMs development (Riding, 2006; Cui et al., 2016; Min et al., 2020).

Silicified cyanobacteria are locally abundant in Proterozoic rocks (Schopf and Klein, 1992), while calcified cyanobacteria are common in units of Cambrian and younger age (Riding, 2006); however, calcified cyanobacteria of Proterozoic age are rare. Our discovery of calcified cyanobacterium *Girvanella* microfossils in the Upper Ediacaran Dengying Formation—the only calcified cyanobacterial taxon identified in the sections we examined—represents a rare occurrence; only a few examples have been previously reported. The earliest confirmed occurrence of calcified cyanobacteria, dated to 750-700 Ma (Knoll et al., 1993), is in columnar stromatolites of the Draken Formation in northwestern Spitsbergen (Swett and Knoll, 1985; Fairchild et al., 1991; Knoll et al., 1993). Two examples of older calcified cyanobacteria (*Girvanella*) have been reported: one from the Little Dal Group in northwestern Canada, with an age of 990-775 Ma (Rainbird et al., 2017; Milton et al., 2017), and the other from the Society Cliffs Formation (Kah and Riding, 2007), dated to 1105 ± 12 Ma to 1109 ± 37 Ma (Turner and Kamber, 2012).

If during much of the Proterozoic seawater carbonate saturation levels were high, as seems likely (Knoll et al., 1993), then why was cyanobacterial calcification so poorly developed in comparison to the Paleozoic? Riding (1994) dubbed this paradox the 'Precambrian Enigma'. The near-absence of calcified cyanobacterial fossils from the interval of Neoproterozoic 'Snowball Earth' glaciation at ~700-570 Ma (Walter et al., 2000) has been attributed to the effects of global cooling (Riding, 2006). Although Mankiewicz (1992) reported that cyanobacteria (including *Girvanella*) are present in Ediacaran-age formations, they claimed that most Ediacaran or older occurrences

10.3389/fmars.2025.1627553

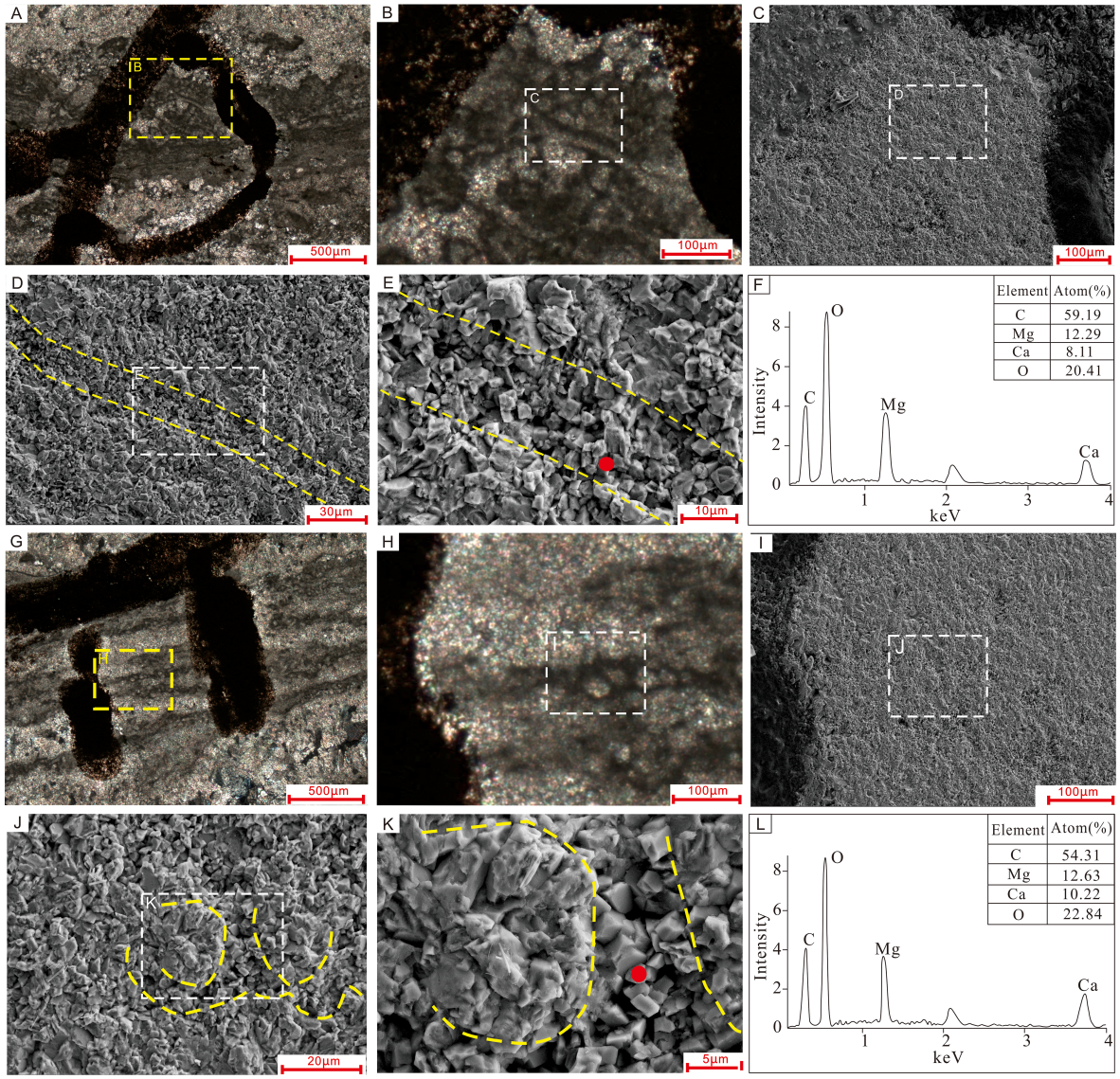


FIGURE 9
Comparison of SEM images, petrographic photos, and EDS chemical spectra of tube-like microfossils in two samples: **(A–F)** Sample I, and **(G–L)** Sample II. **(A, G)** are petrographic microphotographs of thin-sections, with yellow dotted rectangles indicating the positions of SEM images in **(B, H)**. **(C, D)** and **(I, J)** are SEM views of the tube-like microfossils; the white dotted rectangles in **(B, H)** show the positions of images **(C, I)**, respectively. **(E, K)** show the sheaths of the cyanobacteria are composed of euhedral microcrystalline dolomite rhombs with planar crystal faces. Red dotted lines illustrate the outlines of tube-like microfossils, and yellow dots in images **(E, K)** indicate the points analyzed by EDS, with the corresponding chemical spectra shown in **(F, L)**, respectively.

are questionable, representing poorly illustrated and/or described taxa, or taxa from poorly dated strata. Consequently, only a phosphatized fossil assemblage of putatively calcified cyanobacteria from the Gaojiashan Member of the Dengying Formation in the Lijiagou section has been offered as indirect evidence of their existence in the Late Ediacaran (Min et al., 2019, 2020, 2024). As calcified cyanobacteria are typically identified in thin-section (Riding, 1991), our discovery of calcified cyanobacterium *Girvanella* provides direct evidence of such calcified cyanobacteria in the Upper Ediacaran Dengying Formation.

## 5.2 Cyanobacteria in stromatolites of the Ediacaran Period

Precambrian shelf-wide basins commonly feature widespread benthic microbial mats that are almost certainly cyanobacterial in origin (Seilacher and Pflüger, 1994; Schieber, 1999). Some of these mats were preserved in the form of laterally linked carbonate stromatolites (Altermann et al., 2006). Given the ubiquity of cyanobacteria in the terminal Proterozoic (She et al., 2014) and the diverse phosphatized cyanobacterial fossil assemblages discovered in

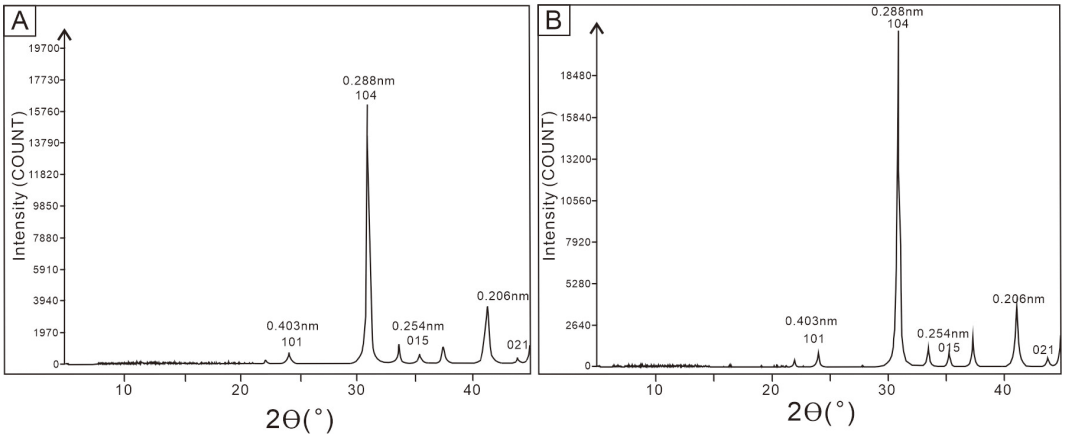


FIGURE 10
XRD patterns of Samples I **(A)** and II **(B)**. Peaks 101, 015 and 021 are superstructure ordering reflections of dolomite.

the upper Gaojiashan Member of the Dengying Formation (Min et al., 2019, 2020, 2024), it is plausible that cyanobacteria played an important role in the formation of microbial mats in the Dengying Formation. Analysis of the microstructures of our samples reveals that *Girvanella*, via its photosynthetic activity, played a key role in the lithification of laminated stromatolites in this stratigraphic unit.

The genus *Girvanella*, a member of the Oscillatoriales family, was initially described by Nicholson and Etheridge (1878). It is characterized by calcareous, thin-walled, variably packed, and unbranched tubular filaments. The tubes, which have a uniform external diameter typically ranging from 7 to 40 μm, are slightly sinuous or irregularly tangled (Riding, 1991; Liu et al., 2016; Min et al., 2020). *Girvanella* occurs nearly continuously from the Cambrian to the Cretaceous and is also present in some recent freshwater environments (Riding, 1991; Arp and Reitner, 2001). It is commonly found in modern tropical to subtropical shallow-marine environments, where it forms skeletal stromatolites, oncolites, crusts on reef surfaces, or distinct microfossils (Riding, 1991; 2000, 2002; Arp and Reitner, 2001; Vennin et al., 2015).

## 5.3 Episodic calcification of *Girvanella* in the Ediacaran and its significance for paleoceanographic environments

The brownish finely crystalline material that constitutes the thin margins of the tube-like cyanobacterium *Girvanella* was identified via SEM and XRD as dolomite. The microcrystalline dolomite is characterized by euhedral crystal rhombs with flat crystal planes and varying sizes, from less than 2 μm to about 5 μm. *Girvanella* filaments with a dark cylinder of finely crystalline dolomite (visible in thin-section; Figure 5) have also been identified within the Draken Formation, which dates to 750-700 Ma (Knoll et al., 1993). Cyanobacterial microfossils of *Girvanella* microfossils typically exhibit well-preserved tubular morphologies that closely resemble their original living forms. This mode of preservation is attributable to, *in vivo* calcification within their sheaths, driven by CCMs related to photosynthesis (Riding, 2006). $CaCO_3$ precipitates in the sheath, which is composed of extracellular polymeric substances (EPS), resulting in calcification of the organic remains (Riding, 2006). Therefore, the organic matter enclosed within the calcified filament sheaths can reasonably be interpreted as remnants of the original sheath-associated organic material. Aragonite and high-Mg calcite were the primary non- skeletal mineralogies of the Ediacaran Period. Calcified microfossils originally composed of aragonite are prone to dissolution and recrystallization during diagenesis, often obscuring primary features such as tubular morphology and wall structures (Li et al., 2021). A more likely scenario for the presence of microcrystalline dolomite in the sheaths of the *Girvanella* specimens of the present study is early diagenetic dolomitization of a high-Mg calcite precursor that formed via syn-vivo precipitation within the sheaths. CCMs, the development of which is thought to have been triggered by a decrease in atmospheric $CO_2$ and an increase in $O_2$, enhanced photosynthesis and increased the pH within cyanobacterial cells of the extracellular sheath. When $pCO_2$ values fell as low as ~10 times the present atmospheric level (PAL), CCMs were induced to promote *in vivo* $CaCO_3$ precipitation in the sheaths of cyanobacteria. This is the most plausible scenario for the appearance of calcified cyanobacterial fossils in the Precambrian record. From 700 Ma until the end of the Neoproterozoic, atmospheric $pCO_2$ was lower than 10 PAL (Riding, 2006). However, together with slowed development of CCMs and reduced seawater carbonate saturation state due to global cooling, calcification of cyanobacterial sheaths was still not promoted during the 'Snowball Earth' period. The changes in temperature, $pO_2$, and $Ca^{2+}$ concentrations that occurred in the late Neoproterozoic (e.g., Hardie, 2003) likely elevated the seawater carbonate saturation state by the early Cambrian, promoting calcification of sheath cyanobacteria (Riding, 2006). Cyanobacterial calcification events (CCEs; Riding, 1992) were environmentally controlled and reflect periods of elevated carbonate saturation state (Riding, 2000) and altered seawater chemistry and atmospheric composition (Riding, 2006).

Calcium carbonate precipitation in cyanobacterial biofilms due to photosynthetic carbon assimilation is only applicable in settings characterized by low dissolved inorganic carbon (DIC) and high

calcium contents (Arp and Reitner, 2001). The seawater Mg/Ca molar ratio exceeded 4 during most of the Ediacaran Period and gradually declined to around 3 by its end (Li et al., 2021). The sporadic occurrence of the calcified cyanobacterium *Girvanella* in the Dengying Formation may imply abrupt fluctuations in Ediacaran seawater chemistry (e.g., a decline in the Mg/Ca ratio, thereby increasing $Ca^{2+}$ availability), which transiently elevated carbonate saturation levels. Concurrently, the possible rapid development of CCMs may have temporarily enabled the calcification capability of cyanobacteria. Furthermore, the predominance of primary high-Mg calcite mineralization would have favored the preservation of these fossils. Thus, this scenario represents a prelude to the widespread microbial calcification observed in the Cambrian.

## 6 Conclusions

In this study, calcified cyanobacteria, occurring as dolomitic tube-like microfossils previously identified as *Girvanella*, were discovered in four samples from the Deng-2 Member of the Upper Ediacaran Dengying Formation in South China. This discovery fills a gap in the fossil record of calcified cyanobacteria in microbialites of the Ediacaran Period. The predominance of primary high-Mg calcite, that formed via syn-vivo precipitation within the sheaths of *Girvanella* as a potential precursor to microcrystalline dolomite, would have favored the preservation of these fossils. The sporadic occurrence of the calcified cyanobacterium *Girvanella* in the Dengying Formation likely reflects transient episodes of elevated carbonate saturation driven by fluctuations in seawater chemistry. Concurrently, the rapid development of CCMs may have enabled the ephemeral calcification capability of cyanobacteria, collectively foreshadowing the onset of widespread microbial calcification in the Cambrian. Further investigation of calcified cyanobacteria and their host sediment in the Algal Dolostone of the Dengying Formation in South China will be needed to better understand the paleomarine environmental conditions and ages of these cyanobacterial assemblages.

## Data availability statement

The original contributions presented in the study are included in the article/supplementary material. Further inquiries can be directed to the corresponding author.

## Author contributions

YZ: Writing – original draft, Writing – review & editing. GL: Investigation, Methodology, Writing – review & editing. YD: Investigation, Methodology, Writing – review & editing. TA: Writing – review & editing.

## Funding

The author(s) declare financial support was received for the research and/or publication of this article. This work was supported by the National Key Research and Development Program of China (2023YFC2906601) and National Natural Science Foundation of China (Grant No. 42072128, 41972102).

## Conflict of interest

The authors declare that the research was conducted in the absence of any commercial or financial relationships that could be construed as a potential conflict of interest.

## Generative AI statement

The author(s) declare that no Generative AI was used in the creation of this manuscript.

Any alternative text (alt text) provided alongside figures in this article has been generated by Frontiers with the support of artificial intelligence and reasonable efforts have been made to ensure accuracy, including review by the authors wherever possible. If you identify any issues, please contact us.

## Publisher's note



## References

Altermann, W., Kazmierczak, J., Oren, A., and Wright, D. T. (2006). Cyanobacterial calcification and its rock-building potential during 3.5 billion years of Earth history. *Geobiology* 4, 147–166. doi: 10.1111/j.1472-4669.2006.00076.x

Arp, G., and Reitner, J. (2001). Photosynthesis-induced biofilm calcification and calcium concentrations in Phanerozoic oceans. *Science* 292, 1701–1704. doi: 10.1126/science.1057204

Brocks, J. J., Buick, R., Logan, G. A., and Summons, R. E. (2003a). Composition and syngeneity of molecular fossils from the 2.78 to 2.45 billion-year old Mount Bruce Supergroup, Pilbara Craton, Western Australia. *Geochimica Cosmochimica Acta* 67, 4289–4319. doi: 10.1016/S0016-7037(03)00208-4

Brocks, J. J., Buick, R., Summons, R. E., and Logan, G. A. (2003b). A reconstruction of Archean biological diversity based on molecular fossils from the 2.78 to 2.45 billion-year-old Mount Bruce Supergroup, Hamersley Basin, Western Australia. *Geochimica Cosmochimica Acta* 67, 4321–4335. doi: 10.1016/S0016-7037(03)00209-6

Cai, Y. P., Schiffbauer, J. D., Hua, H., and Xiao, S. H. (2011). Morphology and paleoecology of the late Ediacaran tubular fossil *Conotubus hemiannulatus* from the Gaojiashan Lagerstätte of southern Shaanxi Province, South China. *Precambrian Res.* 191, 46–57. doi: 10.1016/j.precamres.2011.09.002

Cohen, K. M., Finney, S. C., Gibbard, P. L., and Fan, J. X. (2023). The ICS international chronostratigraphic chart. *Episodes* 36, 199–204. doi: 10.18814/epiiugs/2013/v36i3/002

Condon, D., Zhu, M. Y., Bowring, S., Wang, W., Yang, A. H., and Jin, Y. G. (2005). U–pb ages from the neoproterozoic doushantuo formation, China. *Science* 308, 95–98. doi: 10.1126/science.1107765

Cui, H., Grazhdankin, D. V., Xiao, S., Peek, S., Rogov, V. I., Bykova, N. V., et al. (2016). Redox-dependent distribution of early macro-organisms: Evidence from the terminal Ediacaran Khatyspyt Formation in Arctic Siberia. *Palaeogeography Palaeoclimatology Palaeoecol.* 461, 122–139. doi: 10.1016/j.palaeo.2016.08.015

Demoulin, C. F., Lara, Y. J., Cornet, L., François, C., Baurain, D., Wilmotte, A., et al. (2019). Cyanobacteria evolution: Insight from the fossil record. *Free Radical Biol. Med.* 140, 206–223. doi: 10.1016/j.freeradbiomed.2019.05.007

Deng, S. W., Fan, R., Li, X., Zhang, S. B., Zhang, B. M., and Lu, Y. Z. (2015). Subdivision and correlation of the Sinia (Ediacaran) System in the Sichuan Basin and its adjacent area. *J. Stratigraphy* 39, 239–254. doi: 10.19839/j.cnki.dcxzz.2015.03.001

Dupraz, C., Reid, R. P., Braissant, O., Decho, A. W., Norman, R. S., and Visscher, P. T. (2009). Processes of carbonate precipitation in modern microbial mats. *Earth-Science Rev.* 96, 141–162. doi: 10.1016/j.earscirev.2008.10.005

Fairchild, I. J., Knoll, A. H., and Swett, K. (1991). Coastal lithofacies and biofacies associated with syndepositional dolomitization and silicification (Draken Formation, Upper Riphean, Svalbard). *Precambrian Res.* 53, 165–197. doi: 10.1016/0301-9268(91)90071-H

Fang, S. X., Hou, F. H., and Dong, Z. X. (2003). Non-stromatolite ecologic system cyanobacteria dolostone in Dengying Formation of Upper-Sinian. *Acta Sedimentologica Sin.* 21, 96–105. doi: 10.3969/j.issn.1000-0550.2003.01.015

Hardie, L. A. (2003). Secular variations in Precambrian seawater chemistry and the timing of Precambrian aragonite seas and calcite seas. *Geology* 31, 785–788. doi: 10.1130/G19657.1

Hoffman, P. F., Abbot, D. S., and Ashkenazy, Y. (2017). Snowball Earth climate dynamics and Cryogenian geology-geobiology. *Sci. Adv.* 3, 1600983. doi: 10.1126/sciadv.1600983

Jansson, C., and Northen, T. (2010). Calcifying cyanobacteria—the potential of biomineralization for carbon capture and storage. *Curr. Opin. Biotechnol.* 21, 365–371. doi: 10.1016/j.copbio.2010.03.017

Jiang, G. Q., Kaufman, A. J., Christie-Blick, N., Zhang, S. H., and Wu, H. C. (2008). Carbon isotope variability across the Ediacaran Yangtze platform in South China: Implications for a large surface-to-deep ocean $\delta^{13}C$ gradient. *Earth Planetary Sci. Lett.* 261, 303–320. doi: 10.1016/j.epsl.2007.07.009

Kah, L. C., and Riding, R. (2007). Mesoproterozoic carbon dioxide levels inferred from calcified cyanobacteria. *Geology* 35, 799–802. doi: 10.1130/G23680A.1

Kamennaya, N. A., Ajo-Franklin, C. M., Northen, T., and Jansson, C. (2012). Cyanobacteria as biocatalysts for carbonate mineralization. *Minerals* 2, 338–364. doi: 10.3390/min2040338

Knoll, A. H., Fairchild, I. J., and Swett, K. (1993). Calcified microbes in Neoproterozoic carbonates; implications for our understanding of the Proterozoic/Cambrian transition. *Palaios* 8, 512–525. doi: 10.2307/3515029

Li, F., Deng, J. T., Kershaw, S., Burne, R., Gong, Q. L., Tang, H., et al. (2021). Microbialite development through the Ediacaran–Cambrian transition in China: Distribution, characteristics, and paleoceanographic implications. *Global Planetary Change* 205, 103586. doi: 10.1016/j.gloplacha.2021.103586

Lin, X. X., Peng, J., Du, L. C., Yan, J. P., and Hou, Z. J. (2017). Characterization of the microbial dolomite of the Upper Sinian Dengying Formation in the Huayuan area of Sichuan Province, China. *Acta Geologica Sinica-English Edition* 91, 806–821. doi: 10.1111/1755-6724.13311

Liu, L. J., Wu, Y. S., Yang, H. J., and Riding, R. (2016). Ordovician calcified cyanobacteria and associated microfossils from the Tarim Basin, Northwest China: systematics and significance. *J. Systematic Palaeontology* 14, 183–210. doi: 10.1080/14772019.2015.1030128

Lochte, K., and Turley, C. M. (1988). Bacteria and cyanobacteria associated with phytodetritus in the deep sea. *Nature* 333, 67–69. doi: 10.1038/333067a0

Mankiewicz, C. (1992). "Proterozoic and Early Cambrian calcareous algae," in *The Proterozoic Biosphere*. Eds. J. W. Schopf and C. Klein (Cambridge: Cambridge University Press), 359–367. doi: 10.1017/CBO9780511601064

Manning-Berg, A. R., Wood, R. S., Williford, K. H., Czaja, A. D., and Kah, L. C. (2019). The taphonomy of Proterozoic microbial mats and implications for early diagenetic silicification. *Geosciences* 9, 9010040. doi: 10.3390/geosciences9010040

Mei, M. X., Riaz, M., Zhang, Z. W., Meng, Q. F., and Hu, Y. (2021). Diversified calcimicrobes in dendrolites of the Zhangxia Formation, Miaolingian Series (Middle Cambrian) of the North China craton. *J. Palaeogeogr.* 10, 8. doi: 10.1186/s42501-021-00087-z

Merz-Preiβ, M. (2000). "Calcification in cyanobacteria," in *Microbial Sediments*. Eds. R. E. Riding and S. M. Awramik (Springer, Berlin), 50–56.

Milton, J. E., Hickey, K. A., Gleeson, S. A., and Friedman, R. M. (2017). New U-Pb constraints on the age of the Little Dal Basalts and Gunbarrel-related volcanism in Rodinia. *Precambrian Res.* 296, 168–180. doi: 10.1016/j.precamres.2017.04.030

Min, X., Hua, H., Liu, L. J., Sun, B., Cui, Z. H., and Dai, Q. K. (2020). A diverse calcified cyanobacteria assemblage in the latest Ediacaran. *Precambrian Res.* 342, 1–10. doi: 10.1016/j.precamres.2020.105669

Min, X., Hua, H., Liu, L. J., Sun, B., Cui, Z. H., and Jiang, T. C. (2019). Phosphatized *Epiphyton* from the terminal Neoproterozoic and its significance. *Precambrian Res.* 331, 1–8. doi: 10.1016/j.precamres.2019.105358

Min, X., Hua, H., Sun, B., Dai, Q. K., and Lou, J. Z. (2024). Phosphatised calcified cyanobacteria at the terminal Ediacaran and the earliest Cambrian transition stage: Response to the paleoenvironment. *Palaeogeography Palaeoclimatology Palaeoecol.* 638, 112057. doi: 10.1016/j.palaeo.2024.112057

Nicholson, H. ,. A., and Etheridge, R. (1878). *A Monograph of the Silurian Fossils of the Girvan District in Ayrshire with Special Reference to Those Contained in the 'Gray Collection'* (Edinburgh: William Blackwood and Sons).

Rainbird, R. H., Rayner, N. M., Hadlari, T., Heaman, L. M., Ielpi, A., Turner, E. C., et al. (2017). Zircon provenance data record lateral extent of pancontinental, early Neoproterozoic rivers and erosional unroofing history of the Grenvillian orogeny. *Geological Soc. America Bull.* 129, 1408–1423. doi: 10.1130/B31695.1

Ridgwell, A., and Zeebe, R. E. (2005). The role of the global carbonate cycle in the regulation and evolution of the Earth system. *Earth Planetary Sci. Lett.* 234, 299–315. doi: 10.1016/j.epsl.2005.03.006

Riding, R. (1991). "Calcified cyanobacteria," in *Calcareous Algae and Stromatolites*. Ed. R. Riding (Springer-Verlag, Berlin), 55–78. doi: 10.1007/978-3-642-52335-9_3

Riding, R. (1992). Temporal variation in calcification in marine cyanobacteria. *J. Geological Soc. London* 149, 979–989. doi: 10.1144/gsjgs.149.6.0979

Riding, R. (1994). "Evolution of algal and cyanobacterial calcification," in *Early Life on Earth*. Ed. S. Bengtson (Columbia University Press, New York), 426–438.

Riding, R. (2000). Microbial carbonates: the geological record of calcified bacterial-algal mats and biofilms. *Sedimentology* 47, 179–214. doi: 10.1046/j.1365-3091.2000.00003.x

Riding, R. (2002). Structure and composition of organic reefs and carbonate mud mounds: concepts and categories. *Earth-Science Rev.* 58, 163–231. doi: 10.1016/S0012-8252(01)00089-7

Riding, R. (2006). Cyanobacterial calcification, carbon dioxide concentrating mechanisms, and Proterozoic – Cambrian changes in atmospheric composition. *Geobiology* 4, 299–316. doi: 10.1111/j.1472-4669.2006.00087.x

Riding, R. (2011). "Calcified cyanobacteria," in *Encyclopedia of Geobiology*. Eds. J. Reitner and V. Thiel (Springer, Dordrecht), 211–223. doi: 10.1007/978-1-4020-9212-1

Schieber, J. (1999). Microbial mats in terrigenous clastics: the challenge of identification in the rock record. *Palaios* 14, 3–12. doi: 10.2307/3515357

Schirrmeister, B. E., Gugger, M., and Donoghue, P. C. (2015). Cyanobacteria and the Great Oxidation Event: evidence from genes and fossils. *Palaeontology* 58, 769–785. doi: 10.1111/pala.12178

Schirrmeister, B. E., Sanchez-Baracaldo, P., and Wacey, D. (2016). Cyanobacterial evolution during the Precambrian. *Int. J. Astrobiology* 15, 187–204. doi: 10.1017/S1473550415000579

Schopf, J. W., and Klein, C. (1992). *The Proterozoic Biosphere: A Multidisciplinary Study* (Cambridge: Cambridge University Press).

Seilacher, A., and Pflüger, F. (1994). "From biomats to benthic agriculture: a biohistoric revolution," in *Biostabilization of Sediments*. Eds. W. E. Krumbein and L. J. Stal (Oldenburg University Press, Oldenburg), 97–105.

She, Z. B., Stronger, P., and Papineau, D. (2014). Terminal Proterozoic cyanobacterial blooms and phosphogenesis documented by the Doushantuo granular phosphorites, II: Microbial diversity and C isotopes. *Precambrian Res.* 251, 62–79. doi: 10.1016/j.precamres.2014.06.004

Shi, Z. J., Wang, Y., Tian, Y. M., and Wang, C. C. (2013). Cementation and diagenetic fluid of algal dolomites in the Sinian Dengying Formation in southeastern Sichuan Basin. *Sci. China Earth Sciences-English Edition* 56, 192–202. doi: 10.1007/s11430-012-4541-x

Sisodia, M. S. (2009). Impact during the Proterozoic Era possibly inundated the Earth with phosphorus. *Int. J. Astrobiology* 8, 187–191. doi: 10.1017/S1473550409004480

Song, J. M., Liu, S. G., Li, Z. W., Luo, P., Yang, D., Sun, W., et al. (2017). Characteristics and controlling factors of microbial carbonate reservoirs in the Upper Sinian Dengying Formation in the Sichuan Basin, China. *Oil Gas Geology* 38, 741–752. doi: 10.11743/ogg20170411

Swett, K., and Knoll, A. H. (1985). Stromatolitic bioherms and microphytolites from the Late Proterozoic Draken Conglomerate Formation, Spitsbergen. *Precambrian Res.* 28, 327–347. doi: 10.1016/0301-9268(85)90037-3

Turner, E. C., James, N. P., and Narbonne, G. M. (2000). Taphonomic control on microstructure in early Neoproterozoic reefal stromatolites and thrombolites. *Palaios* 15, 87–111. doi: 10.1669/0883-1351(2000)015<0087:TCOMIE>2.0.CO;2

Turner, E. C., and Kamber, B. S. (2012). Arctic Bay Formation, Borden Basin, Nunavut (Canada): Basin evoloution, black shale, and dissolved metal systematics in the Mesoproterozoic ocean. *Precambrian Res.* 208-211, 1–18. doi: 10.1016/j.precamres.2012.03.006

Turner, E. C., Narbonne, G. M., and James, N. P. (1993). Neoproterozoic reef microstructures from the Little Dal Group, northwestern Canada. *Geology* 21, 259–262. doi: 10.1130/0091-7613(1993)021<0259:NRMFTL>2.3.CO;2

Vennin, E., Olivier, N., Bourillot, R., and Braiser, M. D. (2015). "Microbial sediments," in *Encyclopedia of Geobiology*. Eds. J. Reitner and V. Thiel (Springer, Dordrecht), 567–584. doi: 10.1007/978-3-662-04036-2

Walter, M. R., Veevers, J. J., Calver, C. R., Gorjan, P., and Hill, A. C. (2000). Dating the 840–544 Ma Neoproterozoic interval by isotopes of strontium, carbon, and sulfur in seawater, and some interpretative models. *Precambrian Res.* 100, 371–433. doi: 10.1016/S0301-9268(99)00082-0

Woltz, C. R., Porter, S. M., Agić, H., Dehler, C. M., Junium, C. K., Riedman, L. A., et al. (2021). Total organic carbon and the preservation of organic-walled microfossils in Precambrian shale. *Geology* 49, 556–560. doi: 10.1130/G48116.1

Yu, W., Algeo, T. J., Zhou, Q., Du, Y., and Wang, P. (2020). Cryogenian cap carbonate models: A review and critical assessment. *Palaeogeogr. Palaeoclimatol. Palaeoecol.* 552, 109727. doi: 10.1016/j.palaeo.2020.109727

Zhou, J. G., Zhang, J. Y., Deng, H. Y., Chen, Y. N., Hao, Y., Li, W. Z., et al. (2017). Lithofacies paleogeography and sedimentary model of Sinian Dengying Fm in the Sichuan Basin. *Natural Gas Industry B* 4, 217–224. doi: 10.1016/j.ngib.2017.07.023